LETTERS
PUBLISHED ONLINE: 24 JULY 2011 | DOI: 10.1038/NCLIMATE1169
nature climate change

An energetic perspective on the regional response of precipitation to climate change

C. J. Muller[1]* and P. A. O'Gorman[2]

Understanding and predicting the response of the hydrological cycle to climate change is a major challenge with important societal implications. Much progress has been made in understanding the response of global average precipitation by considering the energy balances of the atmosphere and the surface[1–6]. This energetic perspective reveals that changes in temperature, greenhouse gases, aerosols, solar forcing and cloud feedbacks can all affect the global average rate of precipitation[5,7–11]. Local precipitation changes have conventionally been analysed using the water vapour budget, but here we show that the energetic approach can be extended to local changes in precipitation by including changes in horizontal energy transport. In simulations of twenty-first century climate change, this energy transport accounts for much of the spatial variability in precipitation change. We show that changes in radiative and surface sensible heat fluxes are a guide to the local precipitation response over land and at large scales, but not at small scales over the ocean, where cloud and water vapour radiative feedbacks dampen the response. The energetic approach described here helps bridge the gap between our understanding of global and regional precipitation changes. It could be applied to better understand the response of regional precipitation to different radiative forcings, including geo-engineering schemes, as well as to understand the differences between the fast and slow responses of regional precipitation to such forcings.

It is well understood that increases in global average precipitation in response to greenhouse warming are associated with increased latent heating in the atmosphere. The increased latent heating must in turn be balanced by increases in the radiative cooling of the atmosphere together with decreases in the surface sensible heat flux from the surface, so that radiative cooling and precipitation are tightly linked in the global mean[1,3]. This energetic perspective has been used to account for a number of properties of the response of global average precipitation to climate forcings that might otherwise seem mysterious. For example, global average precipitation may decrease if greenhouse-gas concentrations increase but surface temperature is held fixed[3], a transition from an increasing to a decreasing trend in greenhouse-gas concentrations may lead to a temporary further increase in global average precipitation[12], and black-carbon aerosols, which tend to warm the surface, may increase or decrease global average precipitation depending on the level in the atmosphere at which they are added[9]. But the simulated response of the hydrological cycle to climate change is complex and has strong regional variations[13–16]. The water vapour budget has been used to derive expressions relating local changes in precipitation minus evaporation to surface temperature and circulation changes[13–15], with the circulation changes in turn analysed using the moist static energy budget[13] or related to changes in sea surface temperature[17]. Such expressions provide considerable insight, but are difficult to relate to the energetic approach that is useful for global average precipitation. Here, we will introduce an energetic approach for the analysis of local precipitation changes, including simplified scalings analogous to those used in the water vapour budget approach, and seek to answer the question of how tightly linked changes in radiative cooling and precipitation are at sub-global length scales.

At equilibrium, the local and vertically integrated atmospheric energy budget involves a balance between the surface precipitation flux P and the sum of the column-integrated diabatic cooling Q (excluding latent heating) and the column-integrated divergence H of dry static energy fluxes associated with the circulation (see Methods). Taking δ to represent a difference between a future climate and the present climate leads to an expression for the change in the local precipitation rate in terms of the changes in diabatic cooling and dry static energy flux divergence

$$L_c\delta P = \delta Q + \delta H \qquad (1)$$

where L_c denotes the latent heat of condensation (so that all quantities are given in units of $\mathrm{W\,m^{-2}}$). The dry static energy flux divergence contributes positively to the change in local precipitation if the circulation fluxes more dry static energy from the local atmospheric column in the future climate. Changes in diabatic cooling are calculated in terms of changes in the net longwave (LW) and shortwave (SW) radiative loss of the atmospheric column, and the net upward sensible heat flux at the surface (SH): $\delta Q = \delta\mathrm{LW} + \delta\mathrm{SW} - \delta\mathrm{SH}$. The energetic expression (equation (1)) for the change in precipitation may be contrasted with the corresponding expression from the water vapour budget: in place of changes in water vapour flux convergence and evaporation it involves changes in dry static energy flux divergence and diabatic cooling, respectively. The water vapour and energetic budget approaches are equivalent only in regions with no change in the moist static energy flux divergence (as might happen in tropical regions with low gross moist stability).

We apply the energetic perspective on local precipitation change to simulations of climate change with 12 climate models from the third phase of the coupled model intercomparison project (CMIP3), under an emissions scenario (A1B) for greenhouse gases and aerosols, with differences defined as 2081–2100 minus 1981–2000 (see Methods). The spatial pattern of simulated precipitation change is such that the existing pattern of precipitation becomes enhanced (Fig. 1a)[13,14,18] (see Supplementary Fig. S1 for climatological values for 1981–2000). Changes in the dry static energy flux divergence δH do not contribute in the global mean but do account for much of the spatial variability (Fig. 1b). There is generally a negative

[1]Program in Atmospheric and Oceanic Sciences, Princeton University/GFDL, Princeton, New Jersey 08540, USA, [2]Department of Earth, Atmospheric and Planetary Sciences, Massachusetts Institute of Technology, Cambridge, Massachusetts 02139, USA. *e-mail: caroline.muller@noaa.gov.

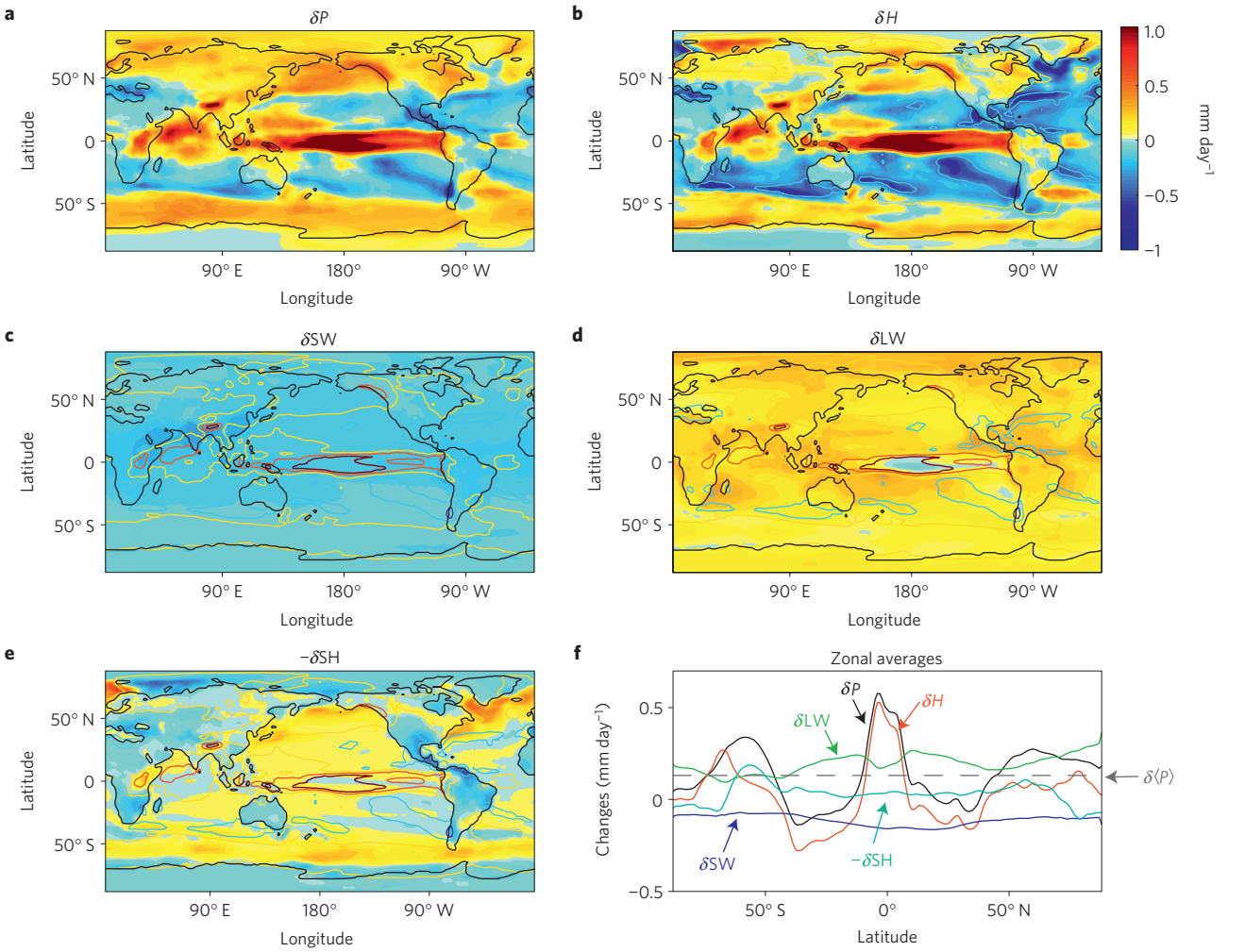

Figure 1 | Spatial pattern of precipitation changes and contributions from the various terms in the energy budget. Here, and in the following figures, the terms in the energy budget are shown in equivalent precipitation units (mm day^{-1}; see Methods for details about the conversion). Annual and multimodel-mean change in **a**, precipitation (δP), **b**, dry static energy flux divergence (δH), **c**, shortwave radiative loss (δSW), **d**, longwave radiative loss (δLW), and **e**, net downward surface sensible heat flux ($-\delta$SH). For ease of comparison, contours of the precipitation change have been added to **b**–**e** (contour interval 0.4 mm day^{-1} from −1 to 1 mm day^{-1}). **f**, Zonal averages and the change in global average precipitation (dashed line).

contribution to the precipitation change from increased shortwave radiative heating (Fig. 1c) (owing primarily to increased solar absorption by water vapour[8]) and a positive contribution from increased longwave radiative cooling (Fig. 1d) (owing primarily to increased temperature offset by increases in greenhouse-gas concentrations[8]). The zonal-mean changes in shortwave and longwave radiative cooling are substantial and offset each other to some extent at all latitudes (Fig. 1f). The surface sensible heat flux contributes positively to the change in global average precipitation in response to greenhouse-gas-driven warming[4,5,19,20], but the sign of the contribution varies regionally (Fig. 1e). In particular, increases in upward sensible heat flux contribute to decreases in precipitation over land regions near the poleward edges of the subtropics.

Interestingly, changes in diabatic cooling tend to dampen the local change in precipitation over the oceans, especially over the tropical Pacific (Supplementary Fig. S2). The global average spatial correlation coefficient of changes in diabatic cooling and precipitation is negative in all the models, with a multimodel-mean value of −0.20, owing to a strong negative correlation of changes in precipitation and net longwave radiative flux at the top of atmosphere (multimodel-mean value of −0.62). Inspection of the spatial patterns of various forcings and feedbacks on the diabatic cooling suggests that the negative correlation must be largely due to cloud and water vapour radiative feedbacks[8], consistent with the negative cloud feedback on precipitation found in earlier studies[5,8,21]. (But note that localized diabatic heating associated with cloud radiative feedbacks will also affect the circulation[13,22] and therefore the export of dry static energy.)

The fact that changes in precipitation and diabatic cooling must be equal in the global mean but are anticorrelated at small scales raises the question of at what length scale do the changes in diabatic cooling and precipitation become tightly linked? To address this question, we calculate the inter-model correlation coefficient between changes in diabatic cooling and precipitation; it is strongly negative over ocean and strongly positive over land (Fig. 2a). (A similar land–ocean contrast has been found for the correlation of precipitation and surface temperature[23].) The positive correlation over land might be expected because the upward sensible heat flux increases in response to dry surface conditions, however the correlation is also positive over land even if only the radiative part of the diabatic cooling is considered. We quantify the scale dependence of the relationship by smoothing the changes in precipitation and diabatic cooling over a range of length scales before calculation of the correlation coefficients. The smoothed fields at a given gridpoint are obtained by spatially

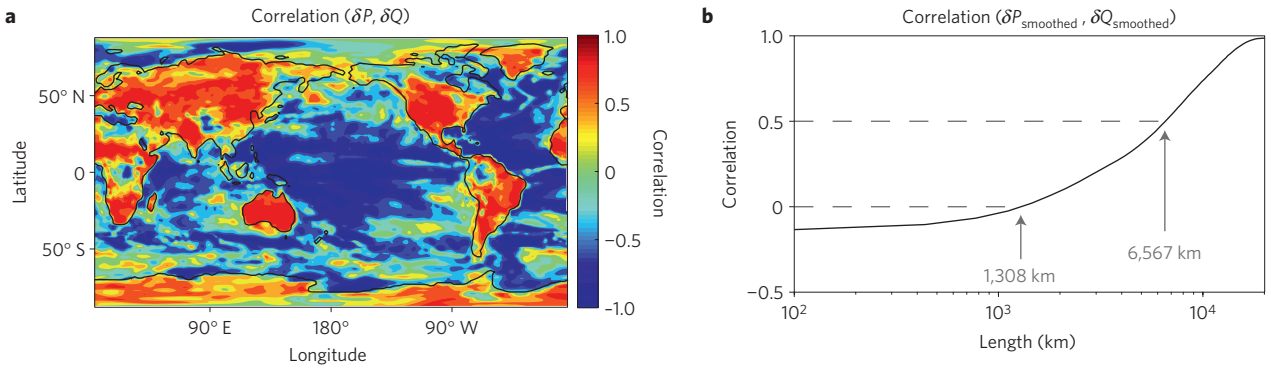

Figure 2 | Inter-model correlation coefficient between the changes in precipitation and diabatic cooling. a, The correlation coefficient between the changes in pointwise precipitation and pointwise diabatic cooling. **b**, Global average of the same correlation coefficient as a function of the length scale in a smoothing filter that is applied to both fields before calculating the correlation coefficient at each point. The global average correlation coefficient transitions from negative to positive at a length scale of ~1,000 km and reaches 0.5 at a length scale of ~7,000 km.

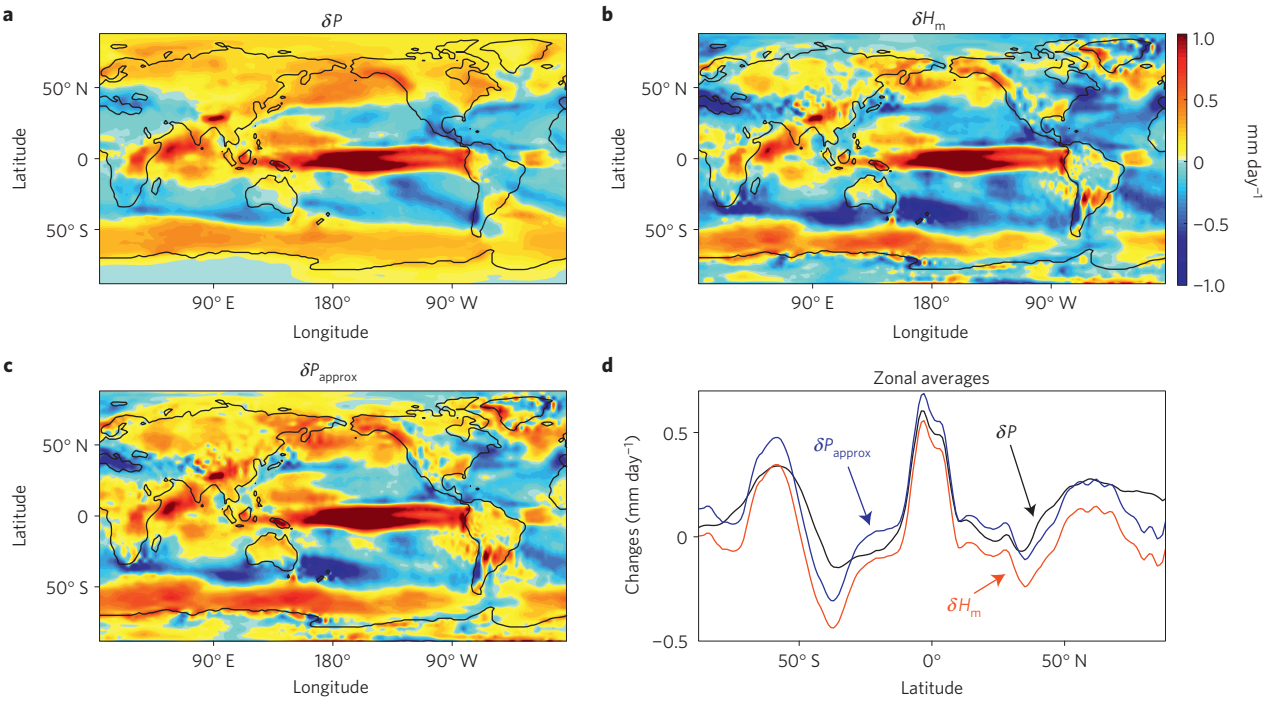

Figure 3 | Annual and multimodel-mean change in precipitation and an approximate expression from energy balance. a, Changes in precipitation δP, **b**, changes in dry static energy flux divergence by mean motions δH_m, and **c**, an approximate expression δP_{approx} for δP (given in equation (2)) that neglects changes in eddy dry static energy flux divergence as well as spatial variations in the change in diabatic cooling; **d**, shows the zonal averages. As in Fig. 1, all values are in mm day^{-1}.

averaging the fields within a given distance of the gridpoint. The global average correlation coefficient changes from negative to positive at a length scale of ~1,000 km, reaches 0.5 at a length scale of ~7,000 km, and asymptotes to one at hemispheric length scales, as expected from global energy balance (Fig. 2b). The implication is that the change in diabatic cooling is generally only a guide to the change in precipitation at relatively large length scales, although they are also tightly linked at small scales over land.

We now focus on the changes in dry static energy flux divergence which dominate the large-scale spatial pattern of precipitation change (Fig. 1a,b,f). In contrast to eddy specific humidity fluxes, which generally increase in magnitude with warming, changes in eddy dry static energy fluxes in the extratropics occur only to the extent that there are changes in the pole-to-Equator temperature gradient or the storm-track winds, and eddy dry static energy fluxes are negligible in the tropics because of weak temperature variations there[24,25]. Consequently, we may neglect the eddy dry static energy flux contribution, but the mean dry static energy flux contribution must clearly be retained (compare Fig. 3a,b). Further neglecting the spatial variations in diabatic cooling results in a much simplified approximate expression δP_{approx} for the change in local precipitation δP as the sum of the change in global average precipitation $\delta\langle P\rangle$ and the change in dry static energy flux divergence by mean motions δH_m

$$L_c\delta P_{approx} = L_c\delta\langle P\rangle + \delta H_m \qquad (2)$$

To the extent that this simplified expression is accurate (Fig. 3c,d), we have related changes in local precipitation to changes in global average precipitation and changes in dry static energy transport by the mean circulation (such as the Hadley, Ferrel, and Walker cells).

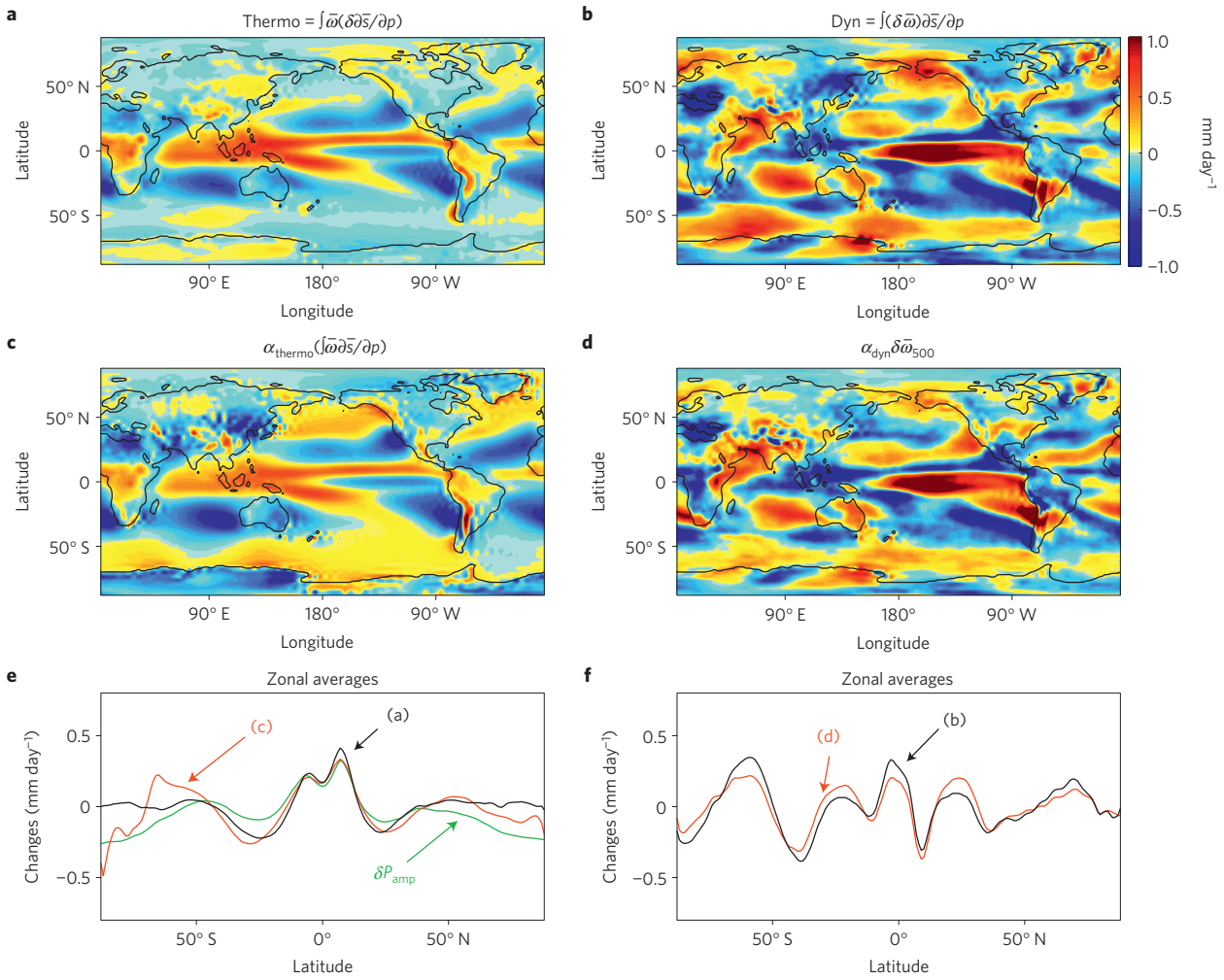

Figure 4 | Annual and multimodel-mean thermodynamic and dynamic contributions to the change in the vertical-advective component of the dry static energy flux divergence. a, Thermodynamic contribution. **b**, Dynamic contribution. **c**, Approximation for the thermodynamic contribution given by equation (5). **d**, Approximation for the dynamic contribution given by equation (6). **e**, Zonal averages for the thermodynamic contributions of **a** and **c** together with an approximation δP_{amp} for the thermodynamic contribution in terms of the mean precipitation distribution (see Methods). **f**, Zonal averages for the dynamic contributions of **b** and **d**. As in Fig. 1, all values are in mm day^{-1}.

The change in dry static energy flux divergence by the mean circulation may be decomposed into components associated with advection across horizontal and vertical gradients of mean dry static energy

$$\delta H_m = \delta\left[\int\left(\bar{\mathbf{u}}\cdot\nabla\bar{s}+\bar{\omega}\frac{\partial\bar{s}}{\partial p}\right)\right]$$

where $\bar{\mathbf{u}}$ is the mean horizontal velocity, $\bar{\omega}$ is the mean vertical velocity in pressure coordinates, $\bar{s}$ is the mean dry static energy, and the integral sign denotes a mass-weighted integral over the atmospheric column (see Methods). The vertical advective component is dominant in the zonal mean because the horizontal advective component has a wave-like character, and it is also dominant in the tropics because of small horizontal gradients of dry static energy there (Supplementary Fig. S3). We focus on the vertical-advective component and decompose it into a dynamic component related to changes in mean vertical velocities ($\delta[\bar{\omega}]$) and a thermodynamic component related to changes in mean dry static stability ($\delta[\partial\bar{s}/\partial p]$),

$$\delta\left[\int\bar{\omega}\frac{\partial\bar{s}}{\partial p}\right]=\int\delta[\bar{\omega}]\frac{\partial\bar{s}}{\partial p}+\int\bar{\omega}\,\delta\left[\frac{\partial\bar{s}}{\partial p}\right] \qquad (3)$$

Similar decompositions into dynamic and thermodynamic changes have been made previously[14,15,26–28]. The thermodynamic component used here depends on changes in the mean thermal stratification and does not assume unchanged relative humidity. It primarily contributes in the tropics, but the dynamical component is important globally and is of a similar magnitude (Fig. 4a,b). Simple approximations are derived that relate the thermodynamic component to the change in temperature (through the change in dry static stability) and the dynamic component to the change in vertical velocity in the mid-troposphere (Methods; Fig. 4c,d). Specifically, the thermodynamic contribution is proportional to the mean vertical advection of dry static energy in the current climate and the dynamic contribution is proportional to the change in mid-tropospheric vertical velocity. The approximation for the dynamic component is particularly simple and accurate; it involves only the change in mean vertical velocity and a scaling constant that may be estimated from the global average dry static stability in the present climate.

The energetic approach to local precipitation is complementary to the conventional water vapour budget approach and links closely to our understanding of changes in global average precipitation and the impacts of radiative forcing. There are several implications

for our understanding of the projected response of regional precipitation to climate change. Within the energetic framework, it is dry static energy transport by the mean circulation that plays a key role in determining the pattern of precipitation change. Shortwave and longwave radiative contributions are also important, but tend to partially offset each other. Cloud and water vapour radiative feedbacks locally dampen the precipitation response over ocean, such that changes in the diabatic cooling are only a guide to the precipitation response for sufficiently large length scales. We have focused on two climates which differ primarily because of greenhouse-gas forcing, but the same approach could also be applied to the response of local precipitation to aerosol forcing and geoengineering schemes, and to the differences between fast and slow responses of precipitation to climate change[29].

Methods

Local energy budget. Making the hydrostatic approximation and neglecting changes in energy and liquid or solid water storage, kinetic energy transports, and work done on the ocean, the time-mean local atmospheric energy budget may be written as[24]

$$L_c P = Q + H \tag{4}$$

where L_c denotes the latent heat of condensation of water vapour (assumed constant and neglecting the latent heat of fusion for simplicity), P surface precipitation rate, Q column-integrated atmospheric diabatic cooling (excluding latent heating), and H column-integrated dry static energy flux divergence. The atmospheric diabatic cooling is calculated as the sum of the net longwave and shortwave radiative fluxes from the column (downwards at the surface and upwards at the top of atmosphere) minus the upward sensible heat flux at the surface, $Q = \mathrm{LW} + \mathrm{SW} - \mathrm{SH}$. The dry static energy flux divergence may be written as a sum of mean and eddy components

$$H = \nabla \cdot \int \bar{\mathbf{u}}\bar{s} + \nabla \cdot \int \overline{\mathbf{u}'s'}$$

where $\int$ denotes mass-weighted vertical integration over the column

$$\int = \int \frac{\mathrm{d}p}{g}$$

$\mathbf{u} = (u, v)$ horizontal velocity, ∇ horizontal gradient, $s = c_p T + gz$ dry static energy, c_p specific heat capacity of air, T temperature, and g acceleration due to gravity. Overbars denote climatological means (12 values at each gridpoint, from January to December, obtained by averaging monthly mean values over 20 years in a given climate), and primes denote departure from the climatological mean. Results are presented by further time averaging to give seasonal or annual statistics (see Supplementary Methods and Fig. S4 for further details of the computation).

Approximations of the dynamic and thermodynamic components. Approximating the fractional change in dry static stability as a constant α_{thermo} leads to an expression for the thermodynamic component (see equation (3)) in terms of the mean vertical-advection of dry static energy in the present climate

$$\int \bar{\omega}\,\delta\left[\frac{\partial \bar{s}}{\partial p}\right] \approx \alpha_{\mathrm{thermo}} \int \bar{\omega}\frac{\partial \bar{s}}{\partial p} \tag{5}$$

with an empirically determined constant factor $\alpha_{\mathrm{thermo}} = 0.1$ that corresponds to a fractional increase in the dry static stability of 3.5% K^{-1} (the multimodel-mean increase in global average surface temperature is 2.9 K). This rate is somewhat lower than expected from a moist-adiabatic stratification (~5% K^{-1} for temperatures and pressures typical of the tropical mid-troposphere[30]). The approximation of the thermodynamic component (equation (5)) is accurate at low latitudes, where the thermodynamic component is important (Fig. 4c,e). Using equation (2), the thermodynamic component may be further approximated as an amplification of current precipitation patterns, $L_c\,\delta P_{\mathrm{amp}} = \alpha_{\mathrm{thermo}}\,L_c\,(P - \langle P \rangle)$, at low latitudes (Fig. 4e). This approximation may be regarded as a version of the 'rich-get-richer' mechanism of precipitation changes[13,14,18]. As the dry static stability is spatially homogeneous, the dynamic component is well approximated as being proportional to the mid-tropospheric change in vertical velocity

$$\int \delta[\bar{\omega}]\frac{\partial \bar{s}}{\partial p} \approx \alpha_{\mathrm{dyn}}\,\delta\,\bar{\omega}|_{500\,\mathrm{hPa}} \tag{6}$$

with an empirically determined constant factor of $\alpha_{\mathrm{dyn}} = -3{,}500\ \mathrm{W\,m^{-2}\,Pa^{-1}\,s}$ (Fig. 4d,f). This factor is close to what would be estimated based on typical values of the dry static stability in the mid-troposphere. The global average value of the dry static stability at 500 hPa is $-50\ \mathrm{m^2\,s^{-2}\,hPa^{-1}}$, and the constant factor α_{dyn} is then estimated as

$$\alpha_{\mathrm{dyn}} \approx \frac{\Delta p}{g}\left.\frac{\partial \bar{s}}{\partial p}\right|_{500\,\mathrm{hPa}} = -4{,}000\ \mathrm{W\,m^{-2}\,Pa^{-1}\,s}$$

where $\Delta p \approx 800$ hPa is a typical pressure depth.

Conversion to equivalent precipitation units. In the figures, the terms in the atmospheric energy budget (in $\mathrm{W\,m^{-2}}$) are converted to equivalent precipitation units (mm $\mathrm{day^{-1}}$) using the conversion factor

$$\frac{86{,}400 \times 1{,}000/\rho_{\mathrm{water}}}{L_c} \approx \frac{1}{29}\ \mathrm{mm\,day^{-1}\,W^{-1}\,m^2}$$

where ρ_{water} denotes the density of liquid water and L_c the latent heat of condensation. The numerator on the left hand side is the unit conversion for precipitation rates from $\mathrm{kg\,s^{-1}\,m^{-2}}$ to mm $\mathrm{day^{-1}}$.

Climate models. Climate change is defined as the difference between 1981 and 2000 in the 20C3M simulations and 2081–2100 in the *Special Report on Emissions Scenarios* (SRES) A1B simulations. The climate models used in the multimodel means are: BCCR-BCM2.0, CGCM3.1(T47), CGCM3.1(T63), CNRM-CM3, ECHAM5/MPI-OM, GFDL-CM2.0, GFDL-CM2.1, GISS-AOM, INM-CM3.0, MIROC3.2(hires), MIROC3.2(medres), and MRI-CGCM2.3.2.

Received 26 April 2011; accepted 28 June 2011; published online 24 July 2011

References

1. Mitchell, J. F. B., Wilson, C. A. & Cunnington, W. M. On CO_2 climate sensitivity and model dependence of results. *Q. J. R. Meteorol. Soc.* **113,** 293–322 (1987).
2. Pierrehumbert, R. T. The hydrologic cycle in deep-time climate problems. *Nature* **419,** 191–198 (2002).
3. Allen, M. R. & Ingram, W. J. Constraints on future changes in climate and the hydrologic cycle. *Nature* **419,** 224–232 (2002).
4. O'Gorman, P. A. & Schneider, T. The hydrological cycle over a wide range of climates simulated with an idealized GCM. *J. Clim.* **21,** 3815–3832 (2008).
5. Stephens, G. L. & Ellis, T. D. Controls of global-mean precipitation increases in global warming GCM experiments. *J. Clim.* **21,** 6141–6155 (2008).
6. Schneider, T., O'Gorman, P. A. & Levine, X. J. Water vapor and the dynamics of climate changes. *Rev. Geophys.* **48,** RG3001 (2010).
7. Lambert, F. H. & Webb, M. J. Dependency of global mean precipitation on surface temperature. *Geophys. Res. Lett.* **35,** L16706 (2008).
8. Previdi, M. Radiative feedbacks on global precipitation. *Environ. Res. Lett.* **5,** 025211 (2010).
9. Ming, Y., Ramaswamy, V. & Persad, G. Two opposing effects of absorbing aerosols on global-mean precipitation. *Geophys. Res. Lett.* **37,** L13701 (2010).
10. Wild, M. & Liepert, B. The Earth radiation balance as driver of the global hydrological cycle. *Environ. Res. Lett.* **5,** 025203 (2010).
11. Frieler, K., Meinshausen, M., von Deimling, T. S., Andrews, T. & Forster, P. Changes in global-mean precipitation in response to warming, greenhouse gas forcing and black carbon. *Geophys. Res. Lett.* **38,** L04702 (2011).
12. Wu, P., Wood, R., Ridley, J. & Lowe, J. Temporary acceleration of the hydrological cycle in response to a CO_2 rampdown. *Geophys. Res. Lett.* **37,** L12705 (2010).
13. Chou, C. & Neelin, J. D. Mechanisms of global warming impacts on regional tropical precipitation. *J. Clim.* **17,** 2688–2701 (2004).
14. Held, I. M. & Soden, B. J. Robust responses of the hydrological cycle to global warming. *J. Clim.* **19,** 5686–5699 (2006).
15. Seager, R., Naik, N. & Vecchi, G. A. Thermodynamic and dynamic mechanisms for large-scale changes in the hydrological cycle in response to global warming. *J. Clim.* **23,** 4651–4668 (2010).
16. Trenberth, K. E. Changes in precipitation with climate change. *Clim. Res.* **47,** 123–138 (2011).
17. Xie, S. P. *et al.* Global warming pattern formation: sea surface temperature and rainfall. *J. Clim.* **23,** 966–986 (2010).
18. Allan, R. P., Soden, B. J., John, V. O., Ingram, W. & Good, P. Current changes in tropical precipitation. *Environ. Res. Lett.* **5,** 025205 (2010).
19. Lorenz, D. J., DeWeaver, E. T. & Vimont, D. J. Evaporation change and global warming: The role of net radiation and relative humidity. *J. Geophys. Res.* **115,** D20118 (2010).
20. Liepert, B. G. & Previdi, M. Do models and observations disagree on the rainfall response to global warming? *J. Clim.* **22,** 3156–3166 (2010).

21. Sohn, B. J. Cloud-induced infrared radiative heating and its implications for large-scale tropical circulations. *J. Atmos. Sci.* **56,** 2657–2672 (1999).
22. Hoskins, B. J. & Karoly, D. J. The steady linear response of a spherical atmosphere to thermal and orographic forcing. *J. Atmos. Sci.* **38,** 1179–1196 (1981).
23. Trenberth, K. E. & Shea, D. J. Relationships between precipitation and surface temperature. *Geophys. Res. Lett.* **32,** L14703 (2005).
24. Peixoto, J. P. & Oort, A. H. *Physics of Climate* Ch. 13 (Amer. Inst. of Physics, 1992).
25. Trenberth, K. E. & Stepaniak, D. P. Covariability of components of poleward atmospheric energy transports on seasonal and interannual timescales. *J. Clim.* **16,** 3691–3705 (2003).
26. Emori, S. & Brown, S. J. Dynamic and thermodynamic changes in mean and extreme precipitation under changed climate. *Geophys. Res. Lett.* **32,** L17706 (2005).
27. O'Gorman, P. A. & Schneider, T. The physical basis for increases in precipitation extremes in simulations of 21st-century climate change. *Proc. Natl Acad. Sci. USA* **106,** 14773–14777 (2009).
28. Muller, C. J., O'Gorman, P. A. & Back, L. E. Intensification of precipitation extremes with warming in a cloud-resolving model. *J. Clim.* **24,** 2784–2800 (2011).
29. Andrews, T. & Forster, P. M. The transient response of global-mean precipitation to increasing carbon dioxide levels. *Environ. Res. Lett.* **5,** 025212 (2010).
30. Betts, A. K. Thermodynamic constraint on the cloud liquid water feedback in climate models. *J. Geophys. Res.* **92,** 8483–8485 (1987).

Acknowledgements

We acknowledge the modelling groups, the Program for Climate Model Diagnosis and Intercomparison (PCMDI) and the WCRP's Working Group on Coupled Modelling (WGCM) for their roles in making available the WCRP CMIP3 multi-model dataset. Support of this dataset is provided by the Office of Science, US Department of Energy. C.J.M. would like to thank I. Held and G. Vecchi for useful discussions about this work.

Author contributions

C.J.M. and P.A.O. designed the study. C.J.M. performed the analysis and wrote the paper. Both authors discussed the results and edited the manuscript.

Additional information

The authors declare no competing financial interests. Supplementary information accompanies this paper on www.nature.com/natureclimatechange. Reprints and permissions information is available online at http://www.nature.com/reprints. Correspondence and requests for materials should be addressed to C.J.M.